Benchmark study for the application of density functional theory to the prediction of octahedral tilting in perovskites

P. García-Fernández,[1] S. Ghosh,[2] Niall J. English,[2] and J. A. Aramburu[1]
[1]*Departamento de Ciencias de la Tierra y Física de la Materia Condensada, Universidad de Cantabria, Avenida de los Castros s/n, 39005 Santander, Spain*
[2]*SEC Strategic Research Cluster, School of Chemical & Bioprocess Engineering, University College of Dublin, Belfield, Dublin 4, Ireland*
(Received 3 July 2012; published 5 October 2012)

The results of a systematic study of octahedral tilting in oxo- and fluoroperovskites by density functional theory (DFT) calculations are presented and discussed. Eleven perovskites displaying different structural, magnetic, and metallic properties have been studied by means of nine exchange-correlation functionals, ranging from the basic local density approximation to more advanced hybrid functionals, in order to determine the accuracy of these methods for the prediction of octahedral rotation angles. Octahedral tilting has attracted much attention lately due to the possibility of using them to trigger improper ferroelectricity and new families of multiferroic materials. We show that all DFT methods tend to overestimate the octahedral rotation angles by approximately 20%, with this quantity being only slightly corrected by hybrids, including, at least, 25% of the Hartree–Fock exchange. We propose a correction to the prediction of these angles based on quantum fluctuations and the anharmonic nature of the energy surface around the minimum but find that it is only important for very small rotation angles appearing in systems like $SrTiO_3$.

DOI: 10.1103/PhysRevB.86.144107 PACS number(s): 61.50.Ah, 71.15.Mb, 31.15.E−

I. INTRODUCTION

Systems with perovskite structure play a major role in current solid-state physics research and material science as electronic, magnetic, and structural degrees of freedom compete with each other to create rich and complicated phase diagrams that can be technologically exploited to build devices.[1–3] During the last two decades, much attention has been focused on the ferroelectric properties of oxides,[4–6] mostly due to their application in such diverse areas as memories, sensors, high-dielectric constant substrates, etc. However, in more recent years, the focus of attention has been shifting toward the study of materials in which other properties interact strongly with ferroelectricity. Foremost of these properties is ferromagnetism, whose interaction with ferroelectricity[1–3,7–10] opens up many new possibilities in the field of information storage, and octahedral tilting,[9–13] another structural instability present in the perovskites (cf. Fig. 1); this is, in fact, much more common than ferroelectric instability in perovskites. Although it is usually assumed that both ferromagnetism[14] and tilting[5,12] compete destructively with ferroelectricity, there are recent reports showing that under adequate circumstances, both properties (see, respectively, Refs. 7, 9–11, and 15) may favor a ferroelectric ground state. Moreover, both properties are of great interest individually as, for example, octahedral tilting plays a very important role in the Earth's mantle material physics under high pressure.[16]

In this field of research, first-principles simulation techniques [i.e., density functional theory (DFT)] have proven themselves extremely useful, being used both as a tool to gain understanding of the underlying physics and as a predictive tool, where new material properties have been measured in the laboratory due to directions from simulation. Although computational methods to calculate ferroelectric properties have been thoroughly tested (see, i.e., Refs. 17–19) and standard recipes to perform simulations in these systems exist [mostly involving the use of the local density approximation (LDA)], the accuracy of different calculation approaches has not been tested systematically for octahedral rotations for a wide range of systems, which may lead to errors when predicting both the geometric and electronic structure in new compounds where these instabilities are important. In fact, in $SrTiO_3$ there are substantial problems to obtain accurately the rotation angle from *ab initio* calculations.[20–23] Taking into account that $SrTiO_3$ is an almost omnipresent system involved in materials in which important new properties have been discovered, like the bidimensional electron gas in $LaAlO_3/SrTiO_3$[24] and improper ferroelectric coupling[11,15] present in $PbTiO_3/SrTiO_3$, this seems troubling. For $SrTiO_3$ plane-wave (PW) LDA calculations[20] lead to a value of the rotation angle Φ of 5.5°, which is more than twice the experimental value (2.1°).[25] As we will see, generalized gradient approximation (GGA) calculations do not significantly help to ameliorate this problem, while several reports in the literature show that the calculated value of Φ improves dramatically with the use of hybrid functionals.[21–23] These results may suggest that using LDA + U, which is frequently employed to set the correct gap and magnetic state of a system, could correct the predicted value of the rotation angle; however, this is not found in calculations.[23] Although the angle calculation problem is well diagnosed in $SrTiO_3$ (*vide supra*), the problem extends to most perovskites. For example, in $CaTiO_3$ and $SrRuO_3$, plain LDA calculations[26,27] provide rotation angles, which are approximately ∼10% larger than their experimental counterparts.[28,29]

In this paper, we systematically study the performance of several DFT functionals in the calculation of various properties of systems with a cubic-perovskite base structure. In particular, we will focus primarily on structural properties, with a strong emphasis on the tilting angles. In order to avoid biases of particular functionals with unique systems or families of systems, we will carry out this benchmark for a database of systems displaying a wide range of properties. In particular,

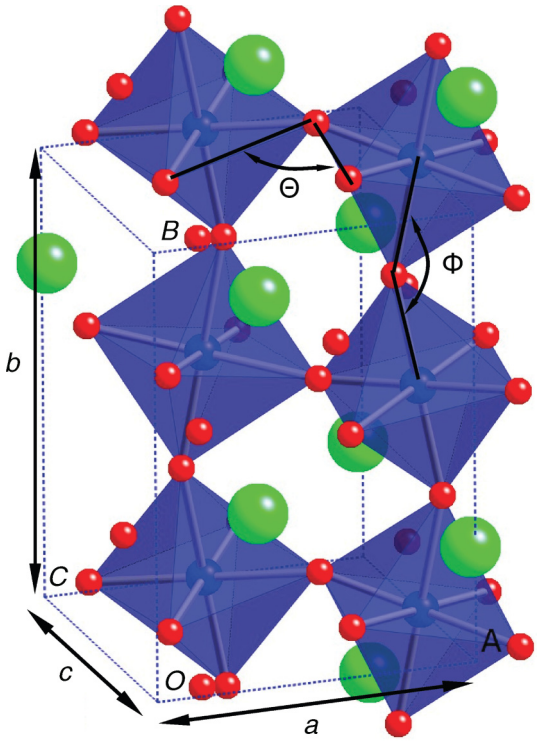

FIG. 1. (Color online) Illustration of the octahedral rotation angles for a typical perovskite in $GdFeO_3$ phase (*Pnma* space group). The tilting angle (ϕ) is obtained from Φ as $\phi = (180 - \Phi)/2$, and the rotation angle (θ) is obtained from Θ as $\theta = (\Theta - 90)/2$.

we will include[28–41] both oxides and fluorides, insulators and metals, and systems with different magnetic behavior, including diamagnetic, antiferromagnetic, and ferromagnetic systems (see summary in Table I). Importantly, since the phase transitions with temperature found in these systems invariably involve, to some degree, an order-disorder component and thermal expansion, neither of which are accounted for in our simulations, all our results will be compared exclusively with low-temperature experimental data. While most systems displaying octahedral rotations stabilize in the $GdFeO_3$ structure belonging to the orthorhombic *Pnma* space group,[42] we have also chosen some systems like $SrTiO_3$ or $LaAlO_3$, where the lowest-temperature phase is, respectively, tetragonal[25] ($I4/mcm$) and rhombohedral[39] ($R3c$), to cover all possibilities. In this way, the studied compounds involve systems that are important in Earth sciences (like $MgSiO_3$ or $NaMgF_3$), common substrates/materials in oxide interfaces (like $SrTiO_3$ or $LaAlO_3$), usual electrodes ($SrRuO_3$), manganites ($CaMnO_3$), etc. As indicated above, this study is not centered around ferroelectric systems, which have been studied thoroughly before;[17–19] however, we feel that the study would be lacking if one of these materials was not included. Thus, we have also performed calculations on $PbTiO_3$, which is arguably the system in which the problems of some DFT functionals are more evident.[43,44]

TABLE I. System database used in this work. We classify the systems according to their conductivity as insulators (INS) or metallic (MET) or to their magnetic state as diamagnetic (DIA), ferromagnetic (FM), or antiferromagnetic (AFM).

System	Conductivity	Magnetic state	Glazer tilting group	Space group	Refs.
$MgSiO_3$	INS	DIA	$a^-b^+a^-$	*Pnma*	30
$NaMgF_3$	INS	DIA	$a^-b^+a^-$	*Pnma*	31,32
$CaTiO_3$	INS	DIA	$a^-b^+a^-$	*Pnma*	28
$CaMnO_3$	INS	AFM	$a^-b^+a^-$	*Pnma*	33,34
$SrRuO_3$	MET	FM	$a^-b^+a^-$	*Pnma*	29,37
$KMnF_3$	INS	AFM	$a^-b^+a^-$	*Pnma*	36,38
$SrZrO_3$	INS	DIA	$a^-b^+a^-$	*Pnma*	35
$LaAlO_3$	INS	DIA	$a^-a^-a^-$	$R3c$	39
$PbTiO_3$	INS	DIA	$a^0a^0a^0$	$P4mm$	40,41
$SrTiO_3$	INS	DIA	$a^0a^0c^-$	$I4/mcm$	25

All of these systems will be studied using several DFT functional families. These functionals are usually classified according to their position (rung) on a DFT Jacob's ladder.[45,46] The first step of the ladder is common to most DFT approaches and is occupied by LDA.[47,48] The second one is occupied by GGA functionals[49] and is much more diverse than the first one, spanning popular functionals like Perdew–Becke–Ernzerhof[50] (PBE), the corrected PBE functional[51] (PBEsol), or the more recent Wu–Cohen[18] (WC) one. The third rung contains meta-GGAs that display a dependence on the kinetic energy density,[52] and the fourth includes explicit dependence of individual occupied orbitals, like hybrid functionals.[53,54] In this work we will follow several functional families from the first rung through the second and fourth steps in the ladder, observing how the properties are inherited as we move up. For example, in perovskites, most GGA functionals lead to a systematic error consisting of the prediction of an exaggerated tetragonality (the supertetragonality problem[18,19]), which also has been found in hybrid functionals based on the previous functionals.[19] We will skip rung three of the ladder containing meta-GGA functionals since, as demonstrated by Perdew *et al.*,[51] these functionals yield inferior accuracy in structural parameters compared to typical GGAs like PBEsol at a computational cost similar to hybrids without providing an enhancement on the prediction of the band gap. Moreover, implementation of these functionals is difficult, and they are not present in many of the usual periodic calculation codes. Another final problem that will be scrutinized is the dependence of the results on the amount of mixing with the Hartree–Fock (HF) exchange present in the hybrid functionals. First-principles arguments[54] suggest that this admixture should be close to 25%, producing families like PBE0[55] (the zero indicating the exclusion of semiempirical parameters). On the other hand, functionals with semiempirical parameters favor lower mixings like 20% in the popular three-parameter empirical B3LYP[56,57] or 16% in B1WC.[19] Interestingly, calculations of the magnetic constant seem to require mixings higher than 25%.[58] Thus, in this work we will follow the families LDA→PBE→PBE0, LDA→PBEsol→PBEsol0, LDA→WC→B1WC, and LDA→WCsol→B1WCsol (see Table II).

Apart from the calculations for a large number of typical examples of perovskite systems, we have calculated the structure of the more complicated $AgNbO_3$ perovskite, where ferroelectric and octahedral tilting distortions are combined.[59,60] Recently, a reappraisal of the structural parameters of this

TABLE II. Description of the families of DFT functionals employed in this work. In each row, we include the exchange (EX) and correlation (COR) functionals and the amount of exact exchange mixing (HF).

	PBE0			PBEsol0			B1WC			B1WCsol		
	EX	COR	HF	EX	COR	HF	EX	COR	HF	EX	COR	HF
Rung 1	LDA	LDA	0	LDA	LDA	0	LDA	LDA	0	LDA	LDA	0
Rung 2	PBE	PBE	0	PBEsol	PBEsol	0	WC	PBE	0	WC	PBEsol	0
Rung 3	PBE	PBE	25	PBEsol	PBEsol	25	WC	PBE	16	WC	PBEsol	16

system has been performed[60] by combined experimental/DFT work using GGA functionals. We have recalculated these parameters using some relevant functionals of the above-mentioned families to establish what kind of improvements can be expected from the use of more advanced functionals to determine the precise structure in these kinds of more complicated, challenging systems.

The paper is organized as follows. In Sec. II we provide the computational details of our simulations. In Sec. III we present our results analyzing individually the effect of the functionals on lattice parameters, octahedral rotation angles, and band gap. We finish this section with the analysis of the structure of $AgNbO_3$. In Sec. IV we propose a correction to the prediction of the octahedral rotation angle based on the quantum fluctuations occurring when the energy surface associated with these distortions is flat and anharmonic. Finally, in Sec. V we present our conclusions.

II. COMPUTATIONAL DETAILS

In order to find the geometry and electronic structure of the systems under study at the different levels of calculations, we have used the CRYSTAL (version 09) code.[61] In this method, the Bloch wave functions are represented by a linear combination of atomic orbitals, which, in turn, are expressed as a combination of Gaussian basis functions. Most basis sets[62–73] were taken directly from CRYSTAL's Web page[62] except those for Ca that produced anomalously large errors in the geometries. A summary with the details for all basis sets used in this work can be found in Table III.

Most of the studied systems crystallize in the *Pnma* structure whose lattice parameters are $\sqrt{2} \times 2 \times \sqrt{2}$ larger than the cubic-perovskite unit cell (see Table I). For insulating lattices with this structure, we employed a $8 \times 6 \times 8$ reciprocal space sampling, while for the systems that crystallize in a different structure [$SrTiO_3$ ($I4/mcm$) and $PbTiO_3$ ($P4mm$) and $LaAlO_3$ (R-$3c$)], we employed an $8 \times 8 \times 8$ k-point mesh. In the case of metallic $SrRuO_3$, with *Pnma* structure, we used a $12 \times 10 \times 12$ grid with a secondary Gillat mesh of $24 \times 24 \times 24$. The parameters controlling the accuracy of integration of Coulomb and exchange parameters were set to 9, 9, 9, 9, 18, the energy convergence to 10^{-10} hartree, and an extra-large grid was used for spatial integration of the electron density. Due to the extreme sensibility of the octahedral rotations to the degree of convergence in the geometry optimization, very tight criteria were imposed. In particular, the tolerances for energy, gradients, and displacements were, respectively, 10^{-9} hartree, 0.00003 and 0.00012. Details on the density functionals employed can be found in Table II.

TABLE III. Description of the basis set employed in this work as well as the references where they are described in detail. AE stands for all-electron and PP for pseudopotential. In the contraction column, we follow the usual notation for Gaussian basis sets.

Atom	Type	Electrons	Contraction	References
O	AE	8	8-411g*	63
F	AE	9	7-311g	64
Na	AE	11	8-511g	67
K	AE	19	86-511g*	67
Mg	AE	12	8-511g*	68
Ca	PP	10	PP-311g*	This work
Si	AE	14	66-21g*	69
Sr	PP	10	PP-311g*	70
La	PP	11	PP-34g*	73
	AE	57	976-1111g**	62
Ti	AE	22	86-411g**	66
Mn	AE	25	86-411g**	65
Nb	AE	41	986-31g**	62
Zr	AE	40	976-31g**	62
Ru	AE	44	976-311g**	71
Al	AE	13	85-11g*	72
Ag	AE	47	633-31g**	62

III. RESULTS

A. General remarks

The simulation results are, in general, in good agreement with available experimental data (see Figs. 2–4). For example, metallicity is only found for $SrRuO_3$, all other systems being insulators at $T = 0$ K. Similarly, the prediction of the magnetic state leads to the correct description of experimentally diamagnetic, antiferromagnetic, and ferromagnetic systems. The only exceptions are $CaMnO_3$, where reliable convergences could only be obtained with hybrid functionals, and $LaAlO_3$, whose calculations prove to be very sensitive to the lanthanum basis set. In this last case, while the lattice parameters are correctly described by all tested basis sets, basis sets that lead to accurate values of the tilting angles[62] grossly overestimate the band gap and vice versa: too-small octahedral rotation angles were found for basis sets,[73] leading to reasonable gap values (see below for more details). The main results for lattice parameters, octahedral rotation angles, and band gaps have been summarized in Figs. 2–4, respectively. Other data and numerical tables for all systems can be found in the Supplemental Material.[74]

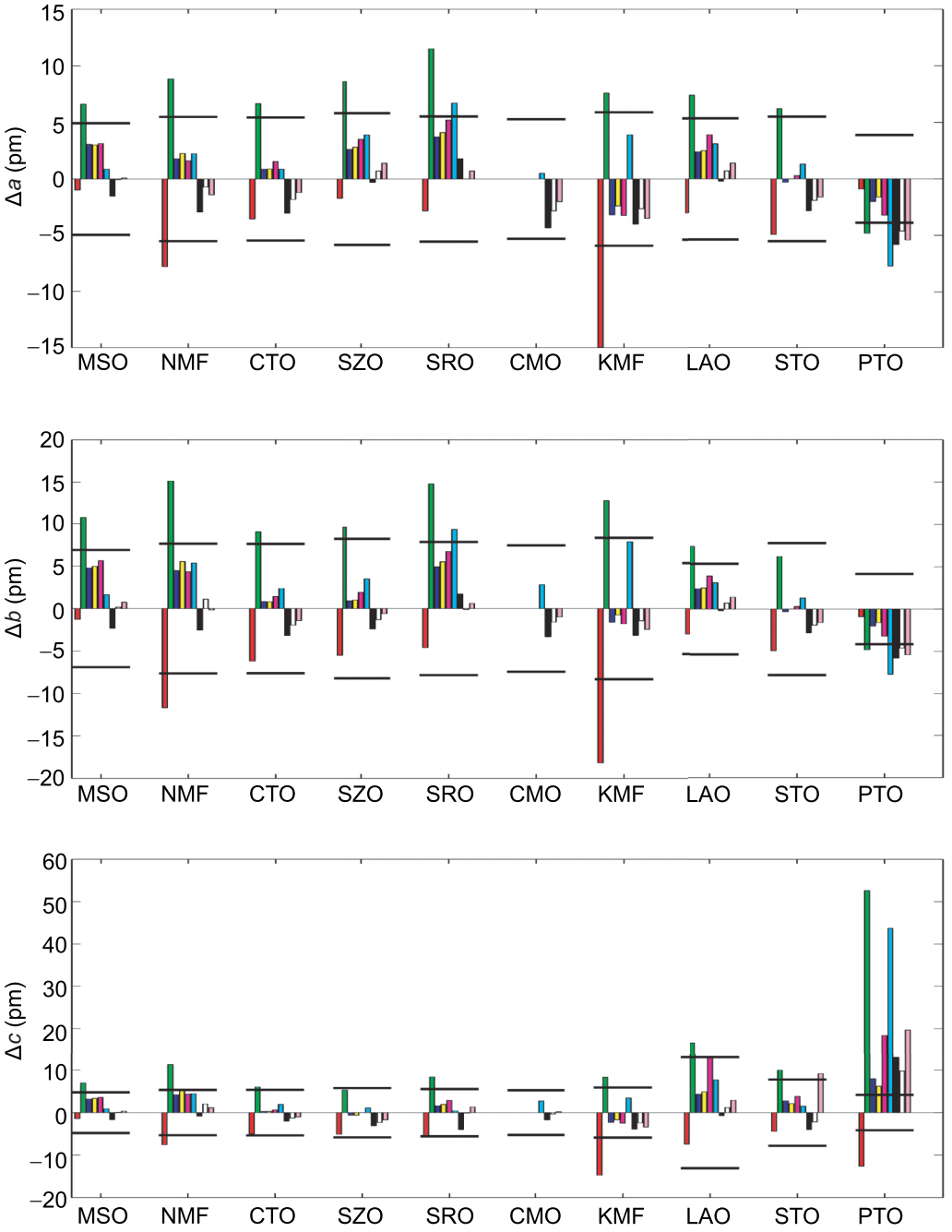

FIG. 2. (Color online) Absolute errors obtained from the comparison of our results with experimental lattice parameters for the systems under study for each of the functionals employed. From left to right, each bar represents LDA, PBE, PBEsol, WC, WCsol, PBE0, PBEsol0, B1WC, and B1WCsol functionals. The horizontal solid lines represent a relative error of 1% in the calculation of the lattice parameter for that system.

B. Equilibrium geometry

In Fig. 2 we present the absolute error made by the studied DFT functionals in the prediction of the lattice parameters a, b, and c for the systems in the dataset employed in this work. As expected, we can see that the errors found for these parameters are very small, usually of a few picometers, and how functionals belonging to different DFT rungs display systematically different behavior. In particular, as is well known, LDA overestimates binding energies and, as a consequence, the lattice parameters are underestimated. On the other hand, the correction of this trend in GGAs is overcompensated, giving rise to cell lengths, which are too large. The inclusion of HF mixing usually represents an improvement with regard to the parent GGA functional, leading to typical absolute errors in the 1- to 3-pm range. Trends within the hybrid functionals are not as clear-cut as with other functionals, probably due to their closeness to the correct results. In any case, results show that DFT can estimate lattice parameters in complex perovskites

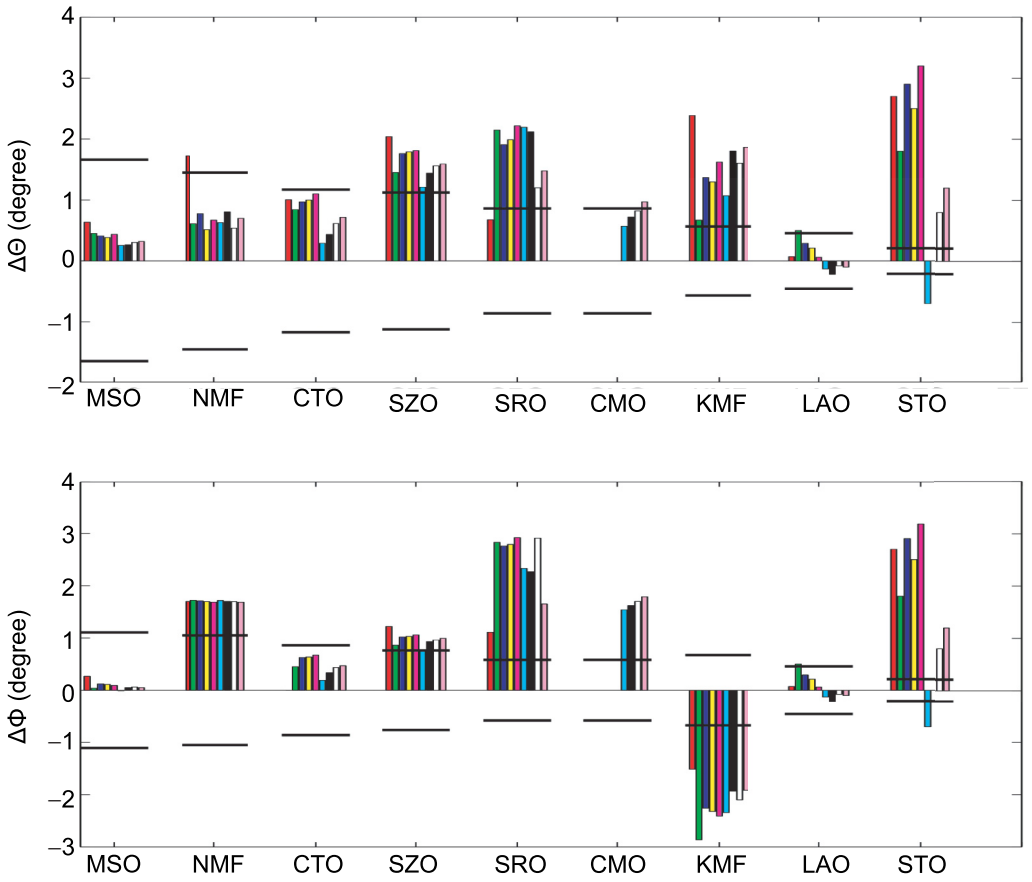

FIG. 3. (Color online) Absolute errors obtained from the comparison of our results with experimental rotation and tilting angles for the systems under study for each of the functionals employed. From left to right, each bar represents LDA, PBE, PBEsol, WC, WCsol, PBE0, PBEsol0, B1WC, and B1WCsol. The horizontal solid lines represent a relative error of 10% in the calculation of the rotation angle for that system.

with relative errors much smaller than 1%, except for LDA and PBE functionals.

When comparing different DFT families (cf. Table II) at the same rung level, we find that the PBE family, including both the pure PBE-GGA and its hybrid sibling PBE0, overestimate the lattice parameters to the greatest extent. This trend is corrected by both the PBEsol and WC families. At the GGA level, both families overestimate the lattice parameters, while hybrids present a bias toward underestimation thereof. When the mean relative error is weighted for each functional (cf. Fig. 5) we can observe that PBEsol, WC, B1WC and B1WCsol perform very similarly with B1WC, yielding the best average

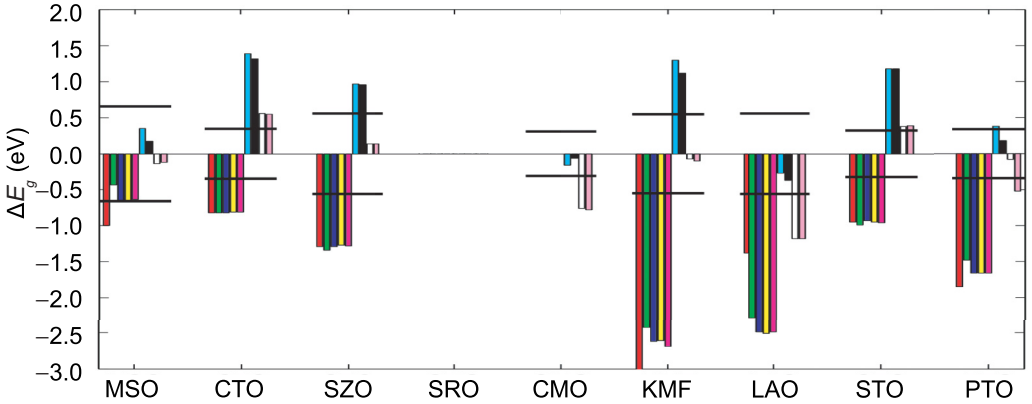

FIG. 4. (Color online) Absolute errors obtained from the comparison of our results with experimental band gaps for the systems under study for each of the functionals employed. From left to right, each bar represents LDA, PBE, PBEsol, WC, WCsol, PBE0, PBEsol0, B1WC, and B1WCsol. The horizontal solid lines represent a relative error of 10% in the calculation of the band gap for that system.

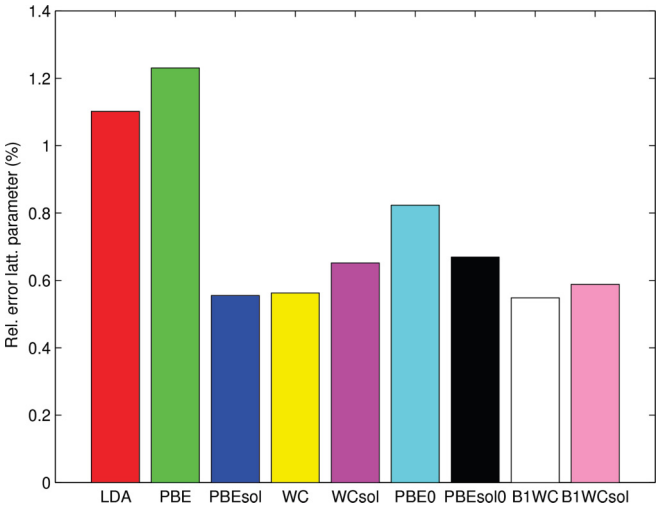

FIG. 5. (Color online) Mean relative error in the calculation of the lattice parameters for each of the functionals.

performance with typical deviations of close to 0.5% relative to the experimental value. The increase of HF mixing from 16% to the theoretically ideal 25% leads to an increase in the mean relative error of 0.1–0.2% due to a decrease of the bond distances with respect to B1WC.

Focusing on particular systems, we see some unusual behavior both in $KMnF_3$ and $PbTiO_3$. In the first case, all functionals except those belonging to the PBE family predict an underestimation of the lattice parameter, particularly LDA where the error is quite large (∼15 pm). The origin of this conduct may reside in the still controversial experimental determination of the low-temperature structure.[36–38] While some works indicate that the system displays a typical Pnma geometry,[36] combined x-ray diffraction and Raman measurements by Kapusta *et al.*[38] point toward a monoclinic structure with $P2_1/m$ space group. Due to these problems, accurate experimental determination of the lattice parameters may be difficult, giving rise to an overestimation of its value and the larger-than-average errors shown in Fig. 1. However, we would like to note our calculations show lower energies for structures calculated at the $P2_1/m$ space group providing support for the experiments carried out by Kapusta *et al.*[38] On the other hand, $PbTiO_3$ remains a difficult system to calculate.[18,19] It is well known that in ferroelectric oxides, GGA functionals tend to elongate the unit cell unrealistically along the main axis of the system leading to the so-called *supertetragonality* problem. In Fig. 2, we observe how all functionals underestimate the in-plane parameter, a (and b, which is equal to a), while the out-of-plane one, c, is overestimated by all except LDA, yielding a tetragonality ratio, c/a, which is much larger than the experimental one. While this effect is particularly marked in the PBE family (including PBE0), all GGAs present it in some degree, and their hybrid derivates usually aggravate the problem. Thus, while LDA is clearly the best-performing functional at this level, WC, PBEsol, and, to a lesser extent, B1WC, are relatively close to experiment with relative errors in the lattice parameters around 1–2%, having been designed to partially correct this issue. It is important to note that supertetragonality only appears in ferroelectric or incipient ferroelectric perovskites, where special issues like giant Born charges are present.[75,76] Indeed, results in Fig. 2 show that GGAs produce good values in general when the systems are far from ferroelectric transitions, like in $SrZrO_3$, $LaAlO_3$, etc.; conversely, $SrTiO_3$, which is close to a ferroelectric transition,[77,78] displays an enhanced c/a ratio vis-à-vis experiment for most of the functionals employed in this work. Calculation of dynamical charges for $SrTiO_3$ and $PbTiO_3$ at the LDA, PBE, and B1WC levels show that they are very similar (within $\Delta q = 0.03$ e) for LDA and PBE and somewhat smaller for the hybrid functionals. Thus, the supertetragonality problem in PBE calculations does not seem related to overestimating the hybridization responsible for dynamical charges but to an underestimation of the elastic constants related to the distortion of the cubic lattice to a tetragonal one.

C. Tilting angles

In the following, we will move the focus to the calculation of octahedral rotation angles. As mentioned in the Introduction, our dataset includes examples of systems presenting different rotation patterns, which can be differentiated using Glazer's notation.[79] In this notation, all rotations can be written using symbols like $a^r b^s c^t$, where a, b, and c are the corresponding octahedral rotation angles around x, y, and z axes, while r, s, and t can be 0, + or −, to indicate, respectively, whether there is no rotation along that axis or that the rotation between two consecutive octahedra is in phase or in phase opposition. The most common rotation pattern in real systems is $a^-b^+a^-$, which is characteristic of the so-called $GdFeO_3$-structure with *Pnma* space group[42] (illustrated in Fig. 1). Experimentally, it is found for all studied systems at low temperature, except in $PbTiO_3$, $LaAlO_3$, $SrTiO_3$, and, perhaps, in $KMnF_3$. The first system does not present octahedral rotation at all ($a^0a^0a^0$), while the next two display, respectively, $a^-a^-a^-$ and $a^0a^0c^-$ Glazer rotation patterns. In the fourth case, experiments[36–38] are inconclusive, whether the structure at low temperature belongs to *Pnma* ($a^-b^+a^-$) or $P2_1/m$ ($a^-b^+c^-$) space groups. Here, we will assume that the structure of this system is *Pnma* and compare data with the corresponding Ref. 36.

In Fig. 3 we compare the *ab initio* data with experimental values for the rotation (θ) and tilting angles (ϕ) in the case of systems of $a^-b^+a^-$ type. For $SrTiO_3$, we plot the rotation angle, while for $LaAlO_3$, we plot half the complementary angle to the Al-O-Al one equivalent to the tilting one. Observing the results (Fig. 3), we find that DFT calculations systematically overestimate the value of the angles by 1–2° and that the mean relative error (Fig. 6) in these quantities, close to 30–40%, is much larger than the one found for lattice parameters. Even so, it must be noted that the typical error in Fig. 3 is close to 10% and that the mean error is significantly increased by the consideration of $SrTiO_3$, which is a critical system in which the experimental rotation angle is very small (2.1°). For example, LDA calculations predict a 4.8° rotation, which is more than twice the experimental value. Correction of the values avoiding $SrTiO_3$ results (also shown in Fig. 6) present a more positive picture with an almost constant relative error of ∼20% across all functionals.

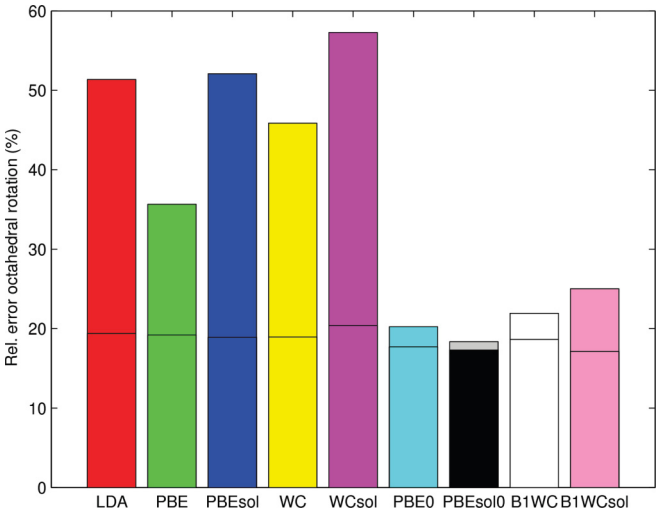

FIG. 6. (Color online) Mean relative error in the calculation of the octahedral rotation angles for each of the functionals. The smaller bar around 20% values is the mean relative error when $SrTiO_3$ has been taken out of the dataset (in PBEsol0 this is represented by a gray bar).

In this work, we consider two main sources of error for the octahedral rotation angles. The first is attributed to the functional themselves: as the changes in electronic structure following a variation in rotation angle that involves bond torsion are more subtle, in the sense of smaller energy variations than the stretching of interatomic distances occurring when lattice parameters are changed, it seems reasonable that calculations are less sensitive to rotations, and the angles are affected by larger relative errors than lattice parameters. The second possible source of error comes from *ab initio* geometries obtained from geometry optimization that can only be directly compared to experiment (without further corrections) when the energy surface around the minimum can be reasonably described by a parabolic well. However, the energy surface associated to octahedral rotations presents, at least, a double-well shape, which can be shallow and far from quadratic. Hence, quantum corrections due to the anharmonic shape of the energy well may lead to better estimations of the tilting angle. We develop and analyze the importance of these corrections in Sec. IV.

Although for lattice parameters we found strong differences between the performance of functionals in the first, second, and fourth Jacob's ladder rungs, in the case of rotations in noncritical cases, they behave in a similar way, providing results that are almost functional independent (Fig. 3). Apart from these initial similarities, we find that LDA usually overestimates angles more than other functionals, while PBE and PBE0 are usually closer to the corresponding experimental values than counterparts in the same rung. It is important to note here that this trend can be physically explained as octahedral rotations, which are strongly coupled to elastic strain[12] and pressure.[13,80] Thus, methods that predict shorter lattice parameters, like LDA, will yield higher rotation angles, while those with longer bonding distances, like PBE, will lead to smaller rotation angles. Graphically, this can be seen in Fig. 6, where average results for each functional over the studied systems are collected. Again, hybrids provide some advantage over the other functional, slightly reducing the errors as their predicted rotation and tilting angles are frequently smaller. However, this correction is typically so small as not to be very significant. The only case in which this correction is important is $SrTiO_3$, where the experimentally measured angle is small, $\theta = 2.1^\circ$, and its prediction by nonhybrid functionals is between 4–5°. Here, inclusion of HF exchange significantly quenches the rotation angle to less than 3°, reducing the differences with experiment. It is important to note that the smallest rotation angles are obtained for functionals with a 25% exchange mixing, yielding angles close to experiment [$\theta(\text{PBE0}) = 1.4^\circ$, $\theta(\text{PBEsol0}) = 2.1^\circ$], while those with the smaller 16% mixing lead to higher values [$\theta(\text{B1WC}) = 2.9^\circ$, $\theta(\text{B1WCsol}) = 3.3^\circ$]. This tendency is general as shown in Fig. 6, where PBE0 and PBEsol0 display smaller errors in angle prediction than B1WC and B1WCsol. This fact could be related to the recently suggested pseudo-Jahn-Teller vibronic origin of tilting.[10,13] In this model the mixing of occupied oxygen or fluorine levels with empty metal levels due to the octahedral rotation is the main reason for energy stabilization. In particular the pseudo-Jahn–Teller[81] contribution to the force constant (K_v) is

$$K_v = -\sum_{i=\text{occ}} \sum_{j=\text{unocc}} \frac{F_{ij}^2}{\Delta_{ij}}. \quad (1)$$

In Eq. (1) i and j run, respectively, over occupied and unoccupied levels, F_{ij} is the pseudo-Jahn-Teller coupling matrix element, and Δ_{ij} is the energy difference between occupied and unoccupied levels. Thus, it seems reasonable that the larger the HF mixing is, the larger Δ_{ij} will be (see below), and the weaker the octahedral rotation instability will be, leading to smaller predicted angles in agreement with the calculation results.

The previous trends are not followed in two systems, $LaAlO_3$ and $KMnF_3$. In the first system, and depending on the basis of the lanthanum ion, it is possible to find tilting angles, which are close to the experimental value (~4.5°) or close to zero. Comparison of the basis parameters does not lead to any simple explanation of this behavior. Finally, in $KMnF_3$ the previously mentioned experimental uncertainly may lead to the unexpected and systematic underestimation of the tilting angle.

D. Band gaps

We have obtained the band gap in our systems by calculating the density of states (DOS) employing a large point sampling in reciprocal space and estimating the difference between the top of the valence band and the bottom of the conducting one. In Fig. 4, we present the error of this band gap as obtained for the different functionals. We find the usual tendencies, which are well characterized in the bibliography. On the one hand, LDA and GGA functionals strongly underestimate the band gap, often by a factor close to 1.5. On the other hand, hybrids are usually much closer to the correct value, but the obtained band-gap is very dependent on the amount of mixing. Average values (cf. Fig. 7) indicate that, for most

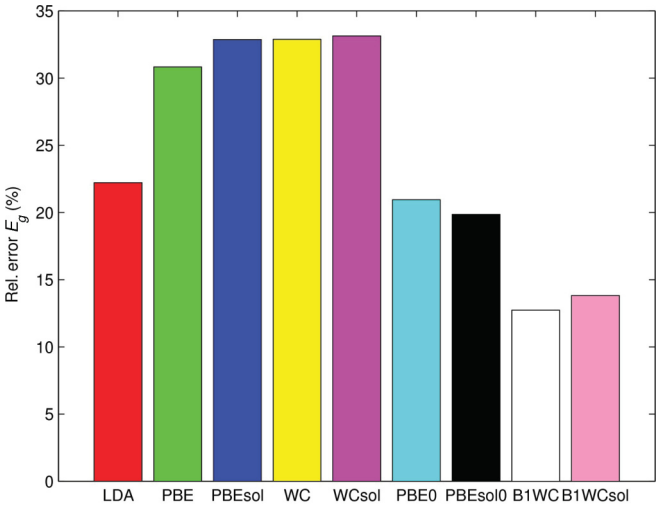

FIG. 7. (Color online) Mean relative error in the calculation of band gap for each of the functionals.

systems, a mixing smaller than the ideal 25% found in PBE0 is necessary for not surpassing the real band gap. This is clearly seen in Fig. 3, where functionals, including 16% HF mixing, are usually much closer to experiment, even though their prediction does not present a clear trend, sometimes overestimating the band gap, like in $CaTiO_3$ and $SrZrO_3$, or underestimating it, like in $CaMnO_3$ or $PbTiO_3$. These results are consistent with recent findings,[82–84] where relatively small HF mixings (≈12.5%) provide excellent band-gap agreement with experiment for $Pb(Ti_{1-x}Ni_x)O_{3-x}$ solid solutions. The only example in which the prediction of hybrids, including 25% HF exchange is more accurate than those including 16%, is in $CaMnO_3$, which is magnetic. This finding may be related to previous reports[58] that indicate that an accurate calculation of the exchange coupling constants using hybrid functionals required large HF exchange mixings, sometimes as high as 35%.

We would finally like to indicate that in $LaAlO_3$ our band gaps are very dependent on the basis on lanthanum as in the case of the tilting angle. However, basis sets that provided realistic angles lead to a gross overestimation of the band gap, while those that involve much smaller octahedral rotation angles lead to underestimated energy excitations that are relatively close to the experimental value.

E. $AgNbO_3$

In order to observe the impact the above factors have on a more complicated system, we have performed calculations on the $AgNbO_3$ perovskite, which has recently received attention due to its large spontaneous polarization and piezoelectric response.[60] However, the presence of both ferroelectric distortion and octahedral rotations complicates the characterization of the geometry of the system, and *ab initio* calculations have been used to complement experiments. Recent synchrotron measurements combined with DFT calculations at the PBE level have allowed the determination of the structure belonging to the $Pmc2_1$ group, leading to a net polarization along the c axis. As seen above, PBE calculations result in an excessive tetragonal deformation of the octahedra in ferroelectrics and cell parameters that are too long. On the other hand, it outperforms other GGA functionals in the prediction of rotation angles. In Table IV, we compare the experimental data and results from PBE calculations extracted from Ref. 60 with our own calculations using LDA (the standard functional used in calculations in ferroelectric systems), a GGA functional, PBE, and, arguably, the best-performing functional of the set, hybrid B1WC.

In order to perform the comparison, we focus on the lattice parameters, the tilting and rotation angles for the two distinct octahedra in the lattice, and the tetragonality of one of them, measured by the distance of the Nb^{5+} ion to its two axial O^{2-} neighbors (Ag-O_1 and Ag-O_2, respectively). Observing Table IV, we first note that LDA performs very well, only being outperformed by PBE or B1WC in the estimation of the rotation angles. From the point of view of qualitative trends, all of the points discussed in the previous sections are present. LDA underestimates the lattice parameters, PBE overestimates them, and B1WC shows mixed results. When it comes to octahedral rotations, LDA clearly overestimates them with relative errors in the 15% range, while this behavior is somewhat corrected for PBE and B1WC, which perform similarly with errors around 5–10%. Finally, regarding tetragonality, we see that all functionals predict an excessive reduction of the Ag-O_1 distance and increase of the Ag-O_2 distance, indicating supertetragonality. This trend is ameliorated for LDA and exaggerated for PBE whose Ag-O_2 distance is overestimated by more than 20 pm. Finally, B1WC partially corrects PBE but is still far from experimental results.

Thus, our results seem to point out that, unless the system involves small gaps, magnetism and/or significant octahedral

TABLE IV. DFT results on $AgNbO_3$ perovskite for selected functionals. Lattice parameters a, b, and c and Ag-O distances are given in angstroms, while Φ and θ angles are in degrees. The signed relative error (in%) with respect to the experimental value is given in parenthesis.

	a	b	c	Φ_1	Φ_2	θ_1	θ_2	Ag-O_1	Ag-O_2
Experiment	15.648	5.552	5.609	9.4	13.1	8.4	8.8	1.943	2.021
LDA	15.478	5.542	5.593	11.6	14.3	9.8	9.7	1.890	2.161
	(−1.1)	(−0.2)	(−0.3)	(23.4)	(9.2)	(16.7)	(10.2)	(−2.7)	(6.9)
PBE (PW)	15.742	5.673	5.743	–	–	–	–	–	–
PBE	15.725	5.712	5.779	10.5	13.3	7.7	7.8	1.885	2.254
	(0.5)	(2.9)	(3.0)	(11.7)	(1.5)	(−8.3)	(−11.4)	(−3.0)	(11.5)
B1WC	15.541	5.600	5.655	10.4	13.2	7.8	7.8	1.872	2.184
	(−0.7)	(0.9)	(0.8)	(10.6)	(0.8)	(−7.1)	(−11.4)	(−3.7)	(8.1)

tilting, calculations on new ferroelectric phases are still better performed using LDA. The best alternative seems to be B1WC, which is well balanced, performing equally well for many kinds of properties and that partially corrects the GGA tendency to supertetragonality although at an increased computational cost. In order to give an estimation of the latter, we would like to indicate that a full geometry optimization at the LDA or GGA level for a *Pnma* cell containing 20 ions in a diamagnetic material like $SrZrO_3$ takes about 5 h using 12 cores in our cluster. The same calculation using a hybrid functional takes approximately three times longer.

IV. EFFECT OF ANHARMONIC CORRECTIONS ON THE MEASUREMENT OF THE OCTAHEDRAL ROTATION ANGLE

In quantum mechanics, the equilibrium geometry of a system is not simply given by the position of the minimum of the energy surface. As illustrated in Fig. 8, when the energy surface deviates from a perfect harmonic oscillator around the stable position, the nuclear wave function is not symmetric around the minimum and the expected position, $Q = \langle\phi|\hat{Q}|\phi\rangle$, deviates from the ideal Q_0. If cubic terms around the minimum are the main responsible for the anharmonic correction, we can write the nuclear movement Hamiltonian as

$$\hat{H} = -\frac{\hbar^2}{2M}\frac{\partial^2}{\partial Q^2} + \frac{1}{2}KQ^2 - AQ^3. \tag{2}$$

Treating the cubic term as a perturbation, we have that the unperturbed energies are

$$E_n = \langle\phi_0|\,\hat{H}\,|\phi_n\rangle = \hbar\omega\left(n + \frac{1}{2}\right), \tag{3}$$

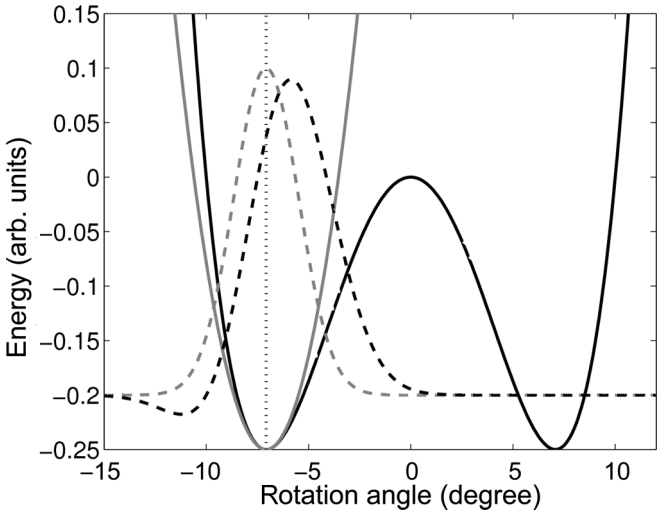

FIG. 8. Qualitative illustration of the quantum fluctuation correction to the expected octahedral rotation angle. The solid black line represents the full double-well energy surface and the black dashed line its ground-state wave function. These can be compared to the ideal harmonic curve associated to the minimum and its ground-state wave function plotted in gray.

and the nuclear wave function corrected to first order is

$$\phi_0' = \frac{1}{\sqrt{N}}\left(\phi_0 - A\sum_n \frac{\langle\phi_0|\,Q^3\,|\phi_n\rangle}{\hbar\omega n}\right). \tag{4}$$

Thus, the correction in the expected value with respect to the minimum is

$$\Delta Q = \langle\phi_0'|\hat{Q}|\phi_0'\rangle = \frac{3\hbar A}{2NM^2\omega^3}. \tag{5}$$

In order to apply these formulae to the octahedral rotation case, we note that the double-well energy surface associated to the effective mode taking us from the ideal cubic geometry to the global minimum can be approximated by

$$V(Q) = -aQ^2 + bQ^4, \tag{6}$$

as illustrated in Fig. 8. There, it can be seen that the quantum correction to the expected angle will always reduce its value as determined using simply the position of the energy surface minimum and will thus be in the right direction taking into account the overestimation shown in Fig. 3. Expansion of Eq. (6) around the minimum to the third order shows that the cubic parameter, A, is

$$A = \pm\sqrt{8ab}. \tag{7}$$

In order to obtain a and b from our *ab initio*, data we employ two conditions: (1) that the minimum following a single effective mode Q leads to the equilibrium rotation and tilting angles predicted using DFT, and (2) that the well depth associated to the double well (Fig. 8) corresponds with the energy difference between the cubic and the stable configurations.

Performing the above calculations, it is found that the correction for most systems is negligible being typically smaller than 0.15°. This result is sensible taking into account that the phase transition from cubic to lower symmetry due to tilting in almost all the systems is $T_c > 800$ K and the stabilization energies are accordingly large. However, in $SrTiO_3$, where the stabilization energy is small, as corresponds with the transition temperature from the tetragonal phase ($I4/mcm$) to the cubic one ($Pm3m$) of 105 K, the correction is much larger. This is shown in Table V, where we see that although the prediction of the rotation angle for LDA and GGA functionals is reduced by ≈0.8° when the correction is included, the final results are still far from the experimental value. However, when the quantum fluctuation is taken into account for the calculations with hybrid functionals, it is found that the prediction of methods including a 25% HF mixing, like PBE0 or PBEsol0, is overcorrected to too small angles, while those including only a 16%, B1WC or B1WCsol, are in excellent agreement with experiment.[35]

Thus, simulations aiming to predict the structural properties of systems with small rotation angles (<5°) should take into account quantum fluctuations in the same way that these perturbations are important in the case of incipient ferroelectric materials.[85] However, in the general case, this correction is very small when compared with the error as a result of determining the position of the minimum of the energy surface.

TABLE V. Corrections to the predicted rotation angle in $SrTiO_3$ when the quantum fluctuations are taken into account. We describe the stabilization energy ΔE given as the difference of energies per Ti ion between the minimum energy of the $Pm3m$ and $I4/mcm$ structures.

	LDA	PBE	PBEsol	WC	WCsol	PBE0	PBEsol0	B1WC	B1WCsol	Experiment
a (Å)	5.458	5.569	5.504	5.507	5.510	5.520	5.479	5.488	5.491	5.507
c (Å)	7.752	7.896	7.823	7.817	7.834	7.811	7.756	7.774	7.888	7.796
ΔE (meV)	5.2					1.5	1.9	5.3	5.4	–
Φ (degree)	4.8	3.9	5.0	4.6	5.3	1.4	2.1	2.9	3.3	2.1
Φ' (degree)	4.0	3.1	4.2	3.8	4.5	0.3	1.0	2.1	2.5	2.1

V. CONCLUSIONS

In this work, we have tested the accuracy of several DFT functional families going from LDA to hybrid passing through various GGAs when predicting structural and electronic properties of oxide and fluoride perovskites. In particular, our results make a strong focus on octahedral rotations, which have been studied intensely in recent years due to their relationship with improper ferroelectricity and the possibility of obtaining new ferromagnetic ferroelectric materials.[6–10] Calculation of rotation and tilting angles involves energy variations that are much smaller than those associated with lattice parameters and is, as a consequence, a more delicate test of the functional's capabilities. We find that all functionals tend to overestimate the octahedral rotation angles in perovskites by about 20%, which is much larger than the typical error (1%) found for bond lengths. The small differences appearing between DFT methods are attributed to the coupling between the rotations and the strain tensor[12] and the prediction of a larger gap in the hybrids, which may affect to covalent terms playing an important role in the origin of tilting.[10,13]

We also showed that care must be exercised when interpreting rotation angles coming from geometry optimization if these angles are small ($<5^\circ$). Similarly to what happens in incipient ferroelectric materials, quantum fluctuations may influence these values importantly. In particular, we show that taking into account the double-well shape associated to the octahedral rotations energy surface, it is possible to write a simple formula that allows for estimating the correction for the expected value of the angle. Although these corrections are negligible for most systems, we find that when applied to $SrTiO_3$, a significantly better prediction is found.

Finally, we find that B1WC is usually the best-performing functional yielding the best lattice parameters and reasonable tilting angles. It must be noted that this functional, including the 16% HF exact exchange, usually leads to better estimates of the electronic gap in these materials than PBE0, which has a tendency to overestimate its value. However, it must be noted that even though B1WC performs better than other GGA and hybrid functionals when calculating properties in ferroelectrics, in the absence of magnetism or strong rotations, LDA is still the reference due to its reduced supertetragonality problem.

ACKNOWLEDGMENTS

We acknowledge economic support from the Spanish Ministerio de Ciencia y Tecnología under Project No. FIS2012-30996 and the Science Foundation Ireland (SFI) Research Frontiers Programme (Reference No. 10/RFP/MTR2868).

[1] N. A. Spaldin and M. Fiebig, Science **309**, 391 (2005).
[2] W. Eerenstein, N. D. Mathur, and J. F. Scott, Nature (London) **442**, 759 (2006).
[3] P. Zubko, S. Gariglio, M. Gabay, P. Ghosez, and J.-M. Triscone, Annu. Rev. Condens. Matter. Phys. **2**, 141 (2011).
[4] M. E. Lines and A. M. Glass, *Principles and Applications of Ferroelectrics and Related Materials* (Oxford University Press, Oxford, 1977).
[5] D. G. Schlom, L.-Q. Chen, C.-B. Eom, K. M. Rabe, S. K. Streiffer, and J.-M. Triscone, Annu. Rev. Mater. Res. **37**, 589 (2007).
[6] M. Dawber, K. M. Rabe, and J. F. Scott, Rev. Mod. Phys. **77**, 1083 (2005).
[7] J. H. Lee and K. M. Rabe, Phys. Rev. Lett. **104**, 207204 (2010).
[8] J. H. Lee, L. Fang, E. Vlahos, X. Ke, Y. W. Jung, L. F. Koukoutis, J.-W. Kim, P. J. Ryan, T. Heeg, M. Roeckerath, V. Goian, M. Bernhagen, R. Uecker, P. C. Hammel, K. M. Rabe, S. Kamba, J. Schubert, J. W. Freeland, D. A. Muller, C. J. Fennie, P. Schiffer, V. Gopalan, E. Johnson-Halperin, and D. G. Schlom, Nature (London) **466**, 954 (2010).
[9] N. A. Benedek and C. J. Fennie, Phys. Rev. Lett. **106**, 107204 (2011).
[10] P. García-Fernández, J. A. Aramburu, and M. Moreno, Phys. Rev. B **83**, 174406 (2011).
[11] E. Bousquet, M. Dawber, N. Stucki, C. Lichtensteiger, P. Hermet, S. Gariglio, J.-M. Triscone, and P. Ghosez, Nature **452**, 732 (2008).
[12] J. M. Rondinelli and N. A. Spaldin, Adv. Mater. **23**, 2263 (2011).
[13] P. García-Fernández, J. A. Aramburu, M. T. Barriuso, and M. Moreno, J. Phys. Chem. Lett. **1**, 647 (2010).
[14] N. A. Hill, J. Phys. Chem. B **104**, 6694 (2000).
[15] P. Aguado-Puente, P. García-Fernández, and J. Junquera, Phys. Rev. Lett. **107**, 217601 (2011).
[16] R. Nomura, H. Ozawa, S. Tateno, K. Hirose, J. Hernlund, S. Muto, H. Ishii, and N. Hiraoka, Nature (London) **473**, 199 (2011).
[17] Ph. Ghosez and J. Junquera, *Handbook of Theoretical and Computational Nanotechnology* (American Scientific Publishers, Stevenson Ranch, CA, 2006), pp. 623–728.
[18] Z. Wu and R. E. Cohen, Phys. Rev. B **73**, 235116 (2006).

[19]D. I. Bilc, R. Orlando, R. Shaltaf, G.-M. Rignanese, J. Iñiguez, and Ph. Ghosez, Phys. Rev. B **77**, 165107 (2008).
[20]N. Sai and D. Vanderbilt, Phys. Rev. B **62**, 13942 (2000).
[21]E. Heifets, E. Kotomin, and V. A. Trepakov, J. Phys.: Condens. Matter **18**, 4845 (2006).
[22]F. El-Mellouhi, E. N. Brothers, M. J. Lucero, and G. E. Scuseria, Phys. Rev. B **84**, 115122 (2011).
[23]M. Verissimo-Alves, P. García-Fernández, D. I. Bilc, P. Ghosez, and J. Junquera, Phys. Rev. Lett. **108**, 107003 (2012).
[24]A. Ohtomo and H. Y. Hwang, Nature (London) **427**, 423 (2004).
[25]E. Courtens, Phys. Rev. Lett. **29**, 1380 (1972).
[26]A. T. Zayak, X. Huang, J. B. Neaton, and K. M. Rabe, Phys. Rev. B **74**, 094104 (2006).
[27]J. M. Rondinelli, N. M. Caffrey, S. Sanvito, and N. A. Spaldin, Phys. Rev. B **78**, 155107 (2008).
[28]S. Sasaki, C. T. Prewitt, J. D. Bass, and W. A. Schulze, Acta Crystallogr. Sec. C **43**, 1668 (1987).
[29]C. W. Jones, P. D. Battle, P. Lightfoot, and W. T. A. Harrison, Acta Crystallogr. Sec. C **45**, 365 (1989).
[30]M. Sugahara, A. Yoshiasa, Y. Komatsu, T. Yamanaka, N. Bolfan-Casanova, A. Nakatsuka, S. Sasaki, and M. Tanaka, Am. Mineral. **91**, 533 (2006).
[31]C. D. Martin, W. A. Crichton, H. Liu, V. Prakapenka, J. Chen, and J. B. Parise, Am. Mineral. **91**, 1703 (2006).
[32]J. Chen, H. Liu, C. D. Martin, J. B. Parise, and D. J. Weidner, Am. Mineral. **90**, 1534 (2005).
[33]E. S. Bozin, A. Sartbaeva, H. Zheng, S. A. Wells, J. F. Mitchell, Th. Proffen, M. F. Thorpe, and S. J. L. Billinge, J. Phys. Chem. Solids **69**, 2146 (2008).
[34]Q. Zhou and B. J. Kennedy, J. Phys. Chem. Solids **67**, 1595 (2006).
[35]B. J. Kennedy, C. J. Howard, and B. C. Chakoumakos, Phys. Rev. B **59**, 4023 (1999).
[36]O. Beckman and K. Knox, Phys. Rev. **121**, 376 (1961).
[37]L. Klein, J. S. Dodge, C. H. Ahn, J. W. Reiner, L. Mieville, T. H. Geballe, M. R. Beasley, and A. Kapitulnik, J. Phys.: Condens. Matter **8**, 10111 (1996).
[38]J. Kapusta, P. Daniel, and A. Ratuszna, Phys. Rev. B **59**, 14235 (1999).
[39]C. J. Howard, B. J. Kennedy, and B. C. Chakoumakos, J. Phys.: Condens. Matter **12**, 349 (2000).
[40]G. Shirane, H. Danner, and P. Pepinsky, Phys. Rev. **105**, 856 (1957).
[41]G. Shirane, P. Pepinsky, and B. C. Frazer, Acta Crystallogr. **9**, 131 (1956).
[42]P. M. Woodward, Acta Crystallogr. Sec. B **533**, 44 (1997).
[43]Z. Wu, R. E. Cohen, and D. J. Singh, Phys. Rev. B **70**, 104112 (2004).
[44]W. Zhong, D. Vanderbilt, and K. M. Rabe, Phys. Rev. Lett. **73**, 1861 (1994).
[45]J. P. Perdew and K. Schmidt, in *Density Functional Theory and Its Application to Materials*, edited by V. Van Doren, C. Van Alsenoy, and P. Geerlings (American Institute of Physics, Melville, New York, 2001), p. 1.
[46]J. Hafner, Comput. Phys. Commun. **177**, 6 (2007).
[47]W. Kohn and L. J. Sham, Phys. Rev. **140**, A1133 (1965).
[48]P. A. M. Dirac, Proc. Cambridge Philos. Soc. **26**, 376 (1930).
[49]R. G. Parr and W. Yang, *Density-Functional Theory of Atoms and Molecules* (Oxford University Press, Oxford, 1989).
[50]J. P. Perdew, K. Burke, and M. Ernzerhof, Phys. Rev. Lett. **77**, 3865 (1996).
[51]J. P. Perdew, A. Ruzsinszky, G. I. Csonka, O. A. Vydrov, G. E. Scuseria, L. A. Constantin, X. Zhou, and K. Burke, Phys. Rev. Lett. **100**, 136406 (2008).
[52]J. Tao, J. P. Perdew, V. N. Staroverov, and G. E. Scuseria, Phys. Rev. Lett. **91**, 146401 (2003).
[53]A. D. Becke, J. Chem. Phys. **98**, 1372 (1993).
[54]J. P. Perdew, M. Ernzerhor, and K. Burke, J. Chem. Phys. **105**, 9982 (1996).
[55]C. Adamo and V. Barone, J. Chem. Phys. **110**, 6158 (1999).
[56]A. D. Becke, J. Chem. Phys. **98**, 5648 (1993).
[57]P. J. Stephens, F. J. Devlin, C. F. Chabalowski, and M. J. Frisch, J. Phys. Chem. **98**, 11623 (1994).
[58]X. Feng and N. M. Harrison, Phys. Rev. B **70**, 092402 (2004).
[59]V. Krayzman and I. Levin, J. Phys.: Condens. Matter **22**, 404201 (2010).
[60]M. Yashima, S. Matsuyama, R. Sano, M. Itoh, K. Tsuda, and D. Fu, Chem. Mater. **23**, 1643 (2011).
[61]R. Dovesi, R. Orlando, B. Civalleri, C. Roetti, V. R. Saunders, and C. M. Zicovich-Wilson, Z. Kristallogr. **220**, 571 (2005).
[62]CRYSTAL Basis Sets Library, http://www.crystal.unito.it/Basis_Sets/Ptable.html (2011).
[63]T. Bredow, K. Jug, and R. A. Evarestov, Phys. Status Solidi B **243**, R10 (2006).
[64]R. Nada, C. R. A. Catlow, C. Pisani, and R. Orlando, Modell. Simul. Mater. Sci. Eng. **1**, 165 (1993).
[65]M. D. Towler, N. L. Allan, N. M. Harrison, V. R. Saunders, W. C. Mackrodt, and E. Apra, Phys. Rev. B **50**, 5041 (1994).
[66]T. Bredow, P. Heitjans, and M. Wilkening, Phys. Rev. B **70**, 115111 (2004).
[67]R. Dovesi, C. Roetti, C. Freyria-Fava, M. Prencipe, and V. R. Saunders, Chem. Phys. **156**, 11 (1991).
[68]L. Valenzano, Y. Noel, R. Orlando, C. M. Zicovich-Wilson, M. Ferrero, and R. Dovesi, Theor. Chem. Acc. **117**, 991 (2007).
[69]R. Nada, C. Catlow, R. Dovesi, and C. Pisani, Phys. Chem. Miner. **17**, 353 (1990).
[70]S. Piskunov, E. Heifets, R. I. Eglitis, and G. Borstel, Comput. Mater. Sci. **29**, 165 (2004).
[71]F. Frechard and P. Sautet, Surf. Sci. **336**, 149 (1995).
[72]M. Catti, G. Valerio, R. Dovesi, and M. Causa, Phys. Rev. B **49**, 14179 (1994).
[73]D. Muñoz, N. M. Harrison, and F. Illas, Phys. Rev. B **69**, 085115 (2004).
[74]See Supplemental Material at http://link.aps.org/supplemental/10.1103/PhysRevB.86.144107 for the full result tables on the studied systems.
[75]W. Zhong, R. D. King-Smith, and D. Vanderbilt, Phys. Rev. Lett. **72**, 3618 (1994).
[76]R. Resta and D. Vanderbilt, in *Physics of Ferroelectrics: A Modern Perspective*, edited by K. Rabe, Ch. H. Anh, and J.-M. Triscone (Springer-Verlag, Berlin, 2007), p. 54.
[77]A. Antons, J. B. Neaton, K. M. Rabe, and D. Vanderbilt, Phys. Rev. B **71**, 024102 (2005).
[78]J. H. Haeni, P. Irvin, W. Chang, R. Uecker, P. Reiche, Y. L. Li, S. Choudhury, W. Tian, M. E. Hawley, B. Craigo, A. K. Tagantsev,

X. Q. Pan, S. K. Streiffer, L. Q. Chen, S. W. Kirchoefer, J. Levy, and D. G. Schlom, Nature (London) **430**, 758 (2004).
[79]A. M. Glazer, Acta Crystallogr. Sec. A **31**, 756 (1975).
[80]J. Zhao, N. L. Ross, and R. J. Angel, Acta Crystallogr Sec. B **60**, 263 (2004).
[81]I. B. Bersuker, *The Jahn-Teller Effect* (Cambridge University Press, Cambridge, 2006).
[82]G. Y. Gou, J. W. Bennett, H. Takenaka, and A. M. Rappe, Phys. Rev. B **83**, 205115 (2011).
[83]H. Xiao, J. Tahir-Kheli, and W. A. Goddard III, J. Phys. Chem. Lett. **2**, 212 (2011).
[84]M. A. L. Marques, J. Vidal, M. J. T. Oliveira, L. Reining, and S. Botti, Phys. Rev. B **83**, 035119 (2011).
[85]W. Zhong and D. Vanderbilt, Phys. Rev. B **53**, 5047 (1996).